IEEE Access
Multidisciplinary | Rapid Review | Open Access Journal

Received August 28, 2021, accepted October 4, 2021, date of publication October 15, 2021, date of current version November 8, 2021.

Digital Object Identifier 10.1109/ACCESS.2021.3120677

Robust ISAR Cross-Range Scaling via Two-Step Rotation Velocity Estimation

BO-HYUN RYU[1], BYUNG-SOO KANG[2], MYUNG-JUN LEE[3], AND KYUNG-TAE KIM[1], (Member, IEEE)

[1]Department of Electrical Engineering, Pohang University of Science and Technology, Pohang 37673, South Korea
[2]Agency for Defense Development, Daejeon 34060, South Korea
[3]Korea Aerospace Research Institute, Daejeon 34133, South Korea

Corresponding author: Kyung-Tae Kim (kkt@postech.ac.kr)

This work was supported by the Energy Cloud Research and Development Program through the National Research Foundation of Korea (NRF) Grant by the Ministry of Science, ICT, under Grant NRF-2019M3F2A1073402.

ABSTRACT To obtain exact size of non-cooperative target in ISAR images, an accurate cross-range scaling (CRS) should be performed. To do this, an image based approach, which exploits two sequential ISAR images based on the scale and rotational relationship between them, has been adopted in the existing ISAR CRS methods. However, they have two major problems: 1) unknown effective rotation center (ERC) of non-cooperative target, and 2) performance degradation owing to the scintillation of two ISAR images. To address these issues, in this paper, we propose a new CRS method, mainly consisting of two steps: 1) coarse estimation of rotation velocity (RV) in range-Doppler (RD) domain after feature extraction and matching, and 2) using the estimate in Step1, fine RV estimation via singular value decomposition (SVD) in range/cross-range (RC) domain. Furthermore, experimental results based on simulated and real measured data are provided to demonstrate the effectiveness of the proposed method.

INDEX TERMS Cross-range scaling, inverse synthetic aperture radar (ISAR), random sample consensus (RANSAC), scale invariant feature transform (SIFT), singular value decomposition (SVD).

I. INTRODUCTION

Inverse synthetic aperture radar (ISAR) can provide two dimensional (2-D) radar image of non-cooperative targets [1]. Because of its advantages (e.g. long-range capability, weather-unaffected, and high-resolution), ISAR has been widely used in military or civilian applications, such as aerial/maritime surveillance [2]–[4]. Especially, high-resolution ISAR image plays an important role in target recognition and classification. In general, the range and cross-range resolution of ISAR image are determined by the frequency bandwidth of transmitted signal and the rotation angle (RA) of a target, respectively [5]. Accordingly, to improve range/cross-range resolution, we need not only a radar system with a wide-frequency band, but also a target's motion with a wide RA. It should be noted that, contrary to the range resolution, cross-range resolution is uncontrollable component because the RA of non-cooperative target is unknown in real-world ISAR imaging.

The associate editor coordinating the review of this manuscript and approving it for publication was Hasan S. Mir.

Generally, 2-D ISAR image can be obtained by classical range-Doppler (RD) processing, which displays target's scattering centers (SCs) in a range-Doppler domain [m-Hz]. In RD processing, the Doppler resolution is related to only the coherent processing interval (CPI). However, even with the same CPIs, RD images of a target can be expanded or compressed in the Doppler domain owing to the target's unknown rotational motion (RM) [6]. This implies that, even for the same target, different RD images can be obtained, which results in critical problem in target recognition and classification. Therefore, RD images should be scaled into a homogenous range/cross-range (RC) images [m-m].

The key issue of cross-range scaling (CRS) is to estimate a correct rotational velocity (RV) of a target, which is the amount of RA divided by CPI. Over decades, a variety of CRS methods have been proposed [7]–[18]. Generally, the methods can be categorized into two groups: signal based method (SBM) and image based method (IBM). In SBMs [7]–[11], the methods exploit chirp rate in the phase of received signal, which is induced by a constant RV of the target. Here, by prominent point processing, a range

TABLE 1. Definition of acronyms used.

Acronym	Explanation	Acronym	Explanation
ISAR	Inverse synthetic aperture radar	RA	Rotation angle
RD	Range-Doppler	SC	Scattering center
CPI	Coherent processing interval	RM	Rotational motion
RC	Range/Cross-range	RV	Rotation velocity
SBM	Signal based method	IBM	Image based method
SNR	Signal-to-noise ratio	ERC	Effective rotation center
FAST	Features from accelerated segment test	PCA	Principal component analysis
PSO	Particle swarm optimization	SVD	Singular value decomposition
NNDR	Nearest neighbor distance ratio	RANSAC	Random sample consensus
IPP	Image projection plane	TM	Translational motion
PRF	Pulse repetition frequency		

bin with a dominant SC is selected and RV can be estimated based on phase information of SCs. However, since the phase signal can be easily corrupted by noise, SBMs often fail in low signal-to-noise (SNR) cases. Typically, some SBMs [10], [11] guarantee a good RV estimation accuracy even in low SNRs. Meanwhile, when multiple SCs exist at the selected and the same range bin, the performance of SBMs can be degraded.

On the other hand, IBMs use the relationship between two sequential ISAR images [12]–[18]. Here, range-compressed data during a certain CPI are divided into two smaller CPIs, and the resulting two sequential ISAR images are obtained by RD processing. In general, most IBMs have been based on image rotation-and-correlation, such that the relative RA between two images and corresponding RV of the target can be estimated. However, it is noteworthy that, IBMs successfully work only when the effective rotation center (ERC) of two images perfectly matches each other. This implies that, exact knowledge of ERC should be known a *priori*. Nonetheless, it is hardly known and very difficult to be estimated in most cases.

To avoid the problem of unknown ERC of the target, Radon transform [16], and 2-D Fourier transform coupled with polar mapping [14] have been applied to two sequential ISAR images. In the former case, the major axes were extracted from both ISAR images via Radon transform, then, RV of the target was estimated by comparing the angle between two axes. On the other hand, the method in [14] utilized the rotation property of Fourier transform. When the polar mapping was applied to 2-D spectrums, rotation in the image domain is converted into translation in the angle domain. Accordingly, RV was deduced such that the correlation between two polar images is maximized. Although the method in [14] and [16] can estimate RV of the target without a *prior* information of ERC, the estimation scheme in both methods is heavily dependent on searching interval in the angle domain. This implies that, the smaller the angular interval, the better the estimation accuracy at the cost of increase of computational complexity, and vice versa.

Meanwhile, recent methods have exploited some feature extraction techniques, adopted from conventional image processing [15], [17], [18]. Owing to its much smaller-dimensional features, compared to the ISAR image itself, feature-extraction based methods could reduce the computational cost of traditional IBMs. Notably, Kang. *et al.* [17] carried out features from accelerated segment test (FAST) for feature extraction, followed by principal component analysis (PCA). Since the PCA is generally used to determine the direction of the largest variance of given data, by comparing two directions obtained from two sequential ISAR images, RV can be estimated without a *priori* information of ERC of the target. However, because an electromagnetic waves returning from the target have a complicated scattering mechanism, the severe scintillation (i.e. a fluctuation of amplitude) of SCs between two sequential ISAR images often occurs in real-world ISAR imaging. In this case, two ERCs of two sequential ISAR images may be different unless the accurate matching between images is carried out. This implies that, the method in [17] cannot guarantee an accurate RV estimation in a practical situation. On the other hand, in [18], scale invariant feature transform (SIFT) [19] was applied to extract non-fluctuating SCs from two sequential ISAR images. Here, the extracted features are matched through two stages: nearest neighbor distance (NNDR) and random sample consensus (RANSAC) [20]. Then, an optimization strategy named particle swarm optimization (PSO) was used to simultaneously find the ERC and RV of the target. Despite its much smaller-dimensional SIFT features, it still requires a huge computation time because PSO iteratively searches the global optimum of ERC and RV of the target.

Motivated by aforementioned problems, this paper presents a new CRS method based on IBM approach. The proposed method is mainly composed of two steps: 1) coarse RV estimation in RD domain and 2) using the estimated RV in Step1, fine RV estimation via singular value decomposition (SVD) in RC domain. First, robust SCs are extracted and matched through SIFT and NNDR, as introduced in [18]. To remove outliers among the matched SCs after implementing NNDR, RANSAC algorithm is adopted and a homography between matched SCs is obtained. Here, RV of the target can be obtained a *priori* in RD domain. Next, by using the estimated RV, matched SCs are scaled into those in RC domain. Then, calculate SVD of the covariance matrix of two matched SCs in RC domain. Accordingly, much accurate RV of the target can be estimated by the trace of a rotation matrix, which is the product of two matrices, each consisting of the left and right singular vectors, respectively.

Notably, the main difference between the proposed method and the existing methods is that, RV estimation is performed twice both in RD domain and RC domain. Generally, in RD domain, the effect of rotation and scaling of two sequential ISAR images is jointly coupled, resulting in the RV estimation in a recursive fashion [12]–[18]. Nonetheless, in this paper, coarse estimation of RV of the target can be conducted as a result of the proposed RANSAC algorithm in RD domain. By using the estimated RV in the previous stage, matched SCs can be scaled into those in RC domain, where two matched SCs have only rotation relationship between them. It is well-known that, since SVD successfully works for the estimation of a rigid body rotation of two objects in conventional image processing [30], much precise RV of the target can be obtained via a simple SVD. Moreover, it should be noted that, in the process of SVD of the covariance matrix, the translation component induced by the unknown ERC of the target is automatically removed. To sum it up, with the proposed two-step RV estimation, we cannot only perform CRS without a *prior* knowledge about ERC of the target, but also can guarantee a good estimation accuracy of RV.

The rest of this paper is organized as follows: Section II describes the scale and rotation relationship between two sequential ISAR images. In Section III, we present the proposed method in detail. The method is composed of two main steps: 1) coarse RV estimation of in RD domain after feature extraction and matching, and 2) fine estimation of RV via SVD in RC domain by using the coarsely estimated RV in Step 1. In Section IV, experimental results are given to validate the efficacy of the proposed method. Here, results of both simulation dataset about point SCs and real measured data of airplane and maritime target are presented. Finally, conclusion is provided in Section V.

Notation – Lower-case (resp. Upper-case) bold letters denote column vectors (resp. matrices). $\mathrm{tr}(\cdot)$, $\det(\cdot)$ and $\|\cdot\|$ denote the matrix trace, matrix determinant and Frobenius norm operators, respectively. $diag\,[a, b]$ denotes the diagonal matrix, which has elements of a and b.

II. PROBLEM FORMULATION

During CPI, ISAR target is confined in a 2-D image projection plane (IPP), illustrated in Fig. 1. Let $P = (x_1, y_1)$ be a SC in a Cartesian coordinate system with the reference point $O_{ref} = \begin{bmatrix} 0 & 0 \end{bmatrix}^T$, where each of coordinates denotes range and cross-range direction, respectively.

In Fig. 1, $R(t)$ is a translational motion (TM), which is the radial change along radar's line of sight, while $\theta(t)$ is a rotational motion that is the change of aspect angle between the line of sight and a target. Here, to obtain focused ISAR image, uniform RM is required because it yields a constant Doppler-frequency shift, which separates SCs in the cross-range direction. In contrast, TM results in envelope misalignment and 1-D phase error in the received data. Similarly, non-uniform RM (i.e. angular acceleration or jerk) induces multi-dimensional phase error. Besides, when a target is involved in a 3-D motion (such as roll, pitch, yaw), the orientation of IPP changes over time. As a result, the uncompensated motions significantly blur the obtained ISAR image. Fortunately, recent methods have been proposed to solve these problems: TM/RM compensation [22]–[27], and selecting suitable imaging frame [28]–[30]. Once aforementioned methods are successfully performed in advance, constant 2-D IPP is detected. Then, ISAR target can be considered as uniformly rotating object.

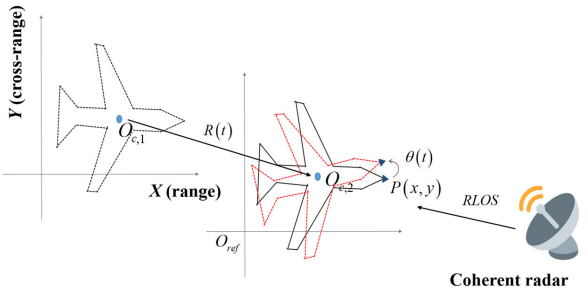

FIGURE 1. Geometry of ISAR imaging.

In ISAR imaging, the range and cross-range resolution are determined as $\Delta r = c/(2B)$ and $\Delta y = \lambda/(2\omega T)$, respectively. Here, c is the speed of light, B is the frequency bandwidth, λ is the wavelength of the carrier frequency, ω is a RV of the target, and T denotes the CPI. When we divide a total CPI into two sub-apertures, two sequential ISAR images, I_1 and I_2, can be obtained by classical RD processing. In particular, two sub-apertures can be overlapped or there may be a gap between them. In addition, when I_1 and I_2 are formed around t_1 and t_2, respectively, the time-difference between I_1 and I_2 becomes $T_m = t_2 - t_1$. Owing to the uniformly rotating target, the aspect angle change between I_1 and I_2 becomes $\Delta\theta = \omega T_m$. Data sets of SCs, $\mathbf{P}_1$ and $\mathbf{P}_2 \in \Re^{2\times L}$, in I_1 and I_2 are expressed in terms of range and Doppler-frequency bins (m, n) [17]:

$$\mathbf{P}_1 = \begin{bmatrix} \mathbf{p}_{1,1} & \mathbf{p}_{1,2} & \cdots & \mathbf{p}_{1,L} \end{bmatrix}, \quad \mathbf{P}_2 = \begin{bmatrix} \mathbf{p}_{2,1} & \mathbf{p}_{2,2} & \cdots & \mathbf{p}_{2,L} \end{bmatrix} \tag{1}$$

where $\mathbf{p}_{i,j} = \begin{bmatrix} m_{i,j} & n_{i,j} \end{bmatrix}^T$ is the location vector of the j-th SC on the i-th image. Here, when the range and CRS factors are provided, I_1 and I_2 in RD domain can be transformed into those in RC domain. Accordingly, data sets of SCs, $\mathbf{P}_1^S$ and $\mathbf{P}_2^S \in \Re^{2\times L}$, in RC domain are expressed as:

$$\mathbf{P}_1^S = \mathbf{S}(\omega)\,\mathbf{P}_1, \quad \mathbf{P}_2^S = \mathbf{S}(\omega)\,\mathbf{P}_2 \tag{2}$$

where $\mathbf{S}(\omega) = diag\,[\eta_r, \eta_c]$ is the scaling matrix and its components are defined as:

$$\eta_r = \frac{c}{2B}, \quad \eta_c = \frac{\lambda f_r}{2M\omega} \tag{3}$$

In (3), f_r is the pulse repetition frequency and M is the number of bursts used to form I_1 and I_2.

Besides, I_1 and I_2 in RC domain have following relationship [16]–[18]:

$$\mathbf{S}(\omega)\left(\mathbf{P}_2 - \mathbf{O}_{C,1}\right) = \mathbf{R}(\Delta\theta)\,\mathbf{S}(\omega)\left(\mathbf{P}_1 - \mathbf{O}_{C,2}\right) \tag{4}$$

where $\mathbf{R}(\Delta\theta)$ is a rotation matrix, which is defined as

$$\mathbf{R}(\Delta\theta) = \begin{bmatrix} \cos(\Delta\theta) & \sin(\Delta\theta) \\ -\sin(\Delta\theta) & \cos(\Delta\theta) \end{bmatrix}. \tag{5}$$

Here, $\mathbf{O}_{C,1} = \begin{bmatrix} x_{c,1} & y_{c,1} \end{bmatrix}^T$ and $\mathbf{O}_{C,2} = \begin{bmatrix} x_{c,2} & y_{c,2} \end{bmatrix}^T$ are the unknown ERCs of the target in I_1 and I_2, respectively. It should be noted that some SCs, which are robust to scintillation between two ISAR images, satisfy the relation in (4). Therefore, ISAR CRS methods based on IBM approach [15], [17], [18] exploited conventional feature extraction techniques (such as SIFT, FAST, and etc.) for feature extraction and RV estimation. Meanwhile, due to unknown ERCs in (4), it becomes a very difficult task to estimate RV of the target.

Motivated by above problem, recent methods in [14]–[18] have been proposed for ISAR CRS without a *prior* knowledge of ERC. Among them, in [18], PCA was used to find the direction of maximum variance of extracted SCs. Here, by finding RA between the major directions obtained from I_1 and I_2, RV can be estimated. Most notably, the method in [17] has a low computation cost through FAST and a suitable cost function, which requires only a few iterations. However, despite of its good computational efficiency, the rotational relationship in (4) holds only when the identical SCs are extracted from both ISAR images, in order to ensure the same ERCs between two ISAR images. Furthermore, in real-world ISAR imaging, when scintillation of SCs between two sequential ISAR images becomes pronounced, the estimated RV by the method in [17] often deviates from the real RV of the target. This implies that, the more the scintillation of SCs, the lower the RV estimation accuracy of the method in [17]. To address the aforementioned problems, we adopt feature extraction via SIFT, followed by feature matching through NNDR and RANSAC. It is noticeable that, matched SCs are robust to scintillation of SCs, a major problem in existing methods.

Besides, the main attribute of the proposed method is that, the RV of the target is found twice in RD domain and RC domain. Since the scaling matrix $\mathbf{S}(\omega)$ is a diagonal matrix and non-singular, (4) can be changed into

$$\begin{aligned} \left(\mathbf{P}_2 - \mathbf{O}_{C,2}\right) &= \mathbf{S}^{-1}(\omega)\,\mathbf{R}(\Delta\theta)\,\mathbf{S}(\omega)\left(\mathbf{P}_1 - \mathbf{O}_{C,1}\right) \\ &= \mathbf{X}(\Delta\theta)\left(\mathbf{P}_1 - \mathbf{O}_{C,1}\right). \end{aligned} \tag{6}$$

In (6), $\mathbf{X}(\Delta\theta)$ can be expressed as

$$\mathbf{X}(\Delta\theta) = \begin{bmatrix} \cos(\Delta\theta) & \gamma\sin(\Delta\theta) \\ -\dfrac{1}{\gamma}\sin(\Delta\theta) & \cos(\Delta\theta) \end{bmatrix}, \tag{7}$$

where $\gamma = {}^{\eta_c}\!/_{\eta_r}$ is the ratio between two scaling factors. It should be noted that, scaling matrix $\mathbf{S}(\omega)$ and rotation matrix $\mathbf{R}(\Delta\theta)$, are jointly coupled through RA as $\mathbf{X}(\Delta\theta)$ in (6), leading to severe difficulty in direct estimation of RV of the target. Accordingly, the optimization in the RD domain has been performed based on a suitable cost function in a recursive fashion [15]–[18]. However, in the RC domain, two sequential ISAR images have only rotation relationship as in (2). To do this, a CRS factor should be provided a *priori*. Meanwhile, in the proposed method, we can estimate RV of the target in the process of RANSAC algorithm, resulting in I_1 and I_2 scaled into those in RC domain. Accordingly, RV of the target can be further refined via simple SVD in the RC domain. In the next section, we present the details of the proposed method.

III. PROPOSED ISAR CRS METHOD

A. FEATURE EXTRACTION AND MATCHING

SIFT is one of widely-used feature extraction techniques in the field of image processing [19]. Especially for rotated and scaled images, SIFT outperforms other feature extraction methods. Hence, for the purpose of ISAR CRS based on IBM approach, SIFT was chosen to find major SCs because two sequential ISAR images in RD domain, I_1 and I_2, which have rotation and scaling relationship. Generally, SIFT consists of following four steps [19]:

(*Step* 1) Scale-space peak selection: Different image scale space can be obtained by variable-scale Gaussian kernel. Multiple key-points are identified by difference-of-Gaussian.

(*Step* 2) Key-point localization: Remove some useless key-points that have low contrast (i.e. sensitive to noise) or are poorly localized along an edge.

(*Step* 3) Orientation assignment: Assign an orientation to each key-point to achieve rotation invariance.

(*Step* 4) Key-point descriptor: Compute a descriptor for each key-point, which has a 128 dimensional vector. To do this, 16×16 window around the key-point is taken. It is divided into $16 = 4 \times 4$ sub-blocks, and in each sub-block, 8-bin orientation histogram is created. Besides, additional measures are taken to achieve rotation or illumination independence.

After applying SIFT algorithm to I_1 and I_2, key-points (i.e. SCs) and corresponding feature descriptors are extracted from each ISAR image. To satisfy the relation in (6), SCs should be matched correctly between two ISAR images. In general, SCs in each image are matched by identifying their nearest neighbors. Suppose that, we have two data sets composed of SIFT descriptors, $\mathbf{A} = [\mathbf{a}_1, \mathbf{a}_2, \ldots, \mathbf{a}_K]^T \in \Re^{128\times K}$ and $\mathbf{B} = \left[\mathbf{b}_1, \mathbf{b}_2, \ldots, \mathbf{b}_Q\right]^T \in \Re^{128\times Q}$ obtained from I_1 and I_2, respectively. The most classical way to compare $\mathbf{A}$ and $\mathbf{B}$ is to calculate an Euclidean distance d [19]:

$$\forall k\; d(q) = \arg\min_k \left\| \mathbf{a}_k - \mathbf{b}_q \right\|, \tag{8}$$

where $k = 1, 2, \ldots K$ and $q = 1, 2, \ldots Q$ are indexes of $\mathbf{A}$ and $\mathbf{B}$, respectively. As a result of (9), all SIFT descriptors in $\mathbf{A}$ and $\mathbf{B}$ can be matched between I_1 and I_2, where each of $\mathbf{A}$ and $\mathbf{B}$ has the smallest d. However, due to noise or some artifacts, the second closest-match may be similar to the closest-match. Moreover, some descriptors in $\mathbf{A}$ may be matched to the same descriptor in $\mathbf{B}$. To this end, we exploit NNDR in [17], [19] to determine a match confidence:

$$\text{NNDR} = {}^{d_1}\!/_{d_2} < G, \tag{9}$$

where d_1 and d_2 are the smallest and the second smallest Euclidean distances between $\mathbf{A}$ and $\mathbf{B}$. The closer the NNDR to 1, the less confident the match. Here, with a pre-defined threshold G, we reject less confident matches where NNDR is larger than the threshold G. Subsequently, P set of SCs are matched between I_1 and I_2.

B. OUTLIER REMOVAL WITH RANSAC ALGORITHM AND COARSE RV ESTIMATION IN RD DOMAIN

Since the matched SCs are used to estimate RV of the target, the matching result directly affects the accuracy of RV estimation. Suppose that we have P sets of matched SCs, $\mathbf{A}_m$ and $\mathbf{B}_m \in \Re^{P\times 3}$ after applying NNDR to $\mathbf{A}$ and $\mathbf{B}$, respectively. To satisfy the relationship in (6), we subtract the mean-values of the locations of the matched SCs after NNDR,

$$\bar{\mathbf{A}}_m = \mathbf{A}_m - \frac{1}{P}\sum_{p=1}^{P}\mathbf{a}_{m,p},\ \bar{\mathbf{B}}_m = \mathbf{B}_m - \frac{1}{P}\sum_{p=1}^{P}\mathbf{b}_{m,p}. \quad (10)$$

Accordingly, $\bar{\mathbf{A}}_m$ and $\bar{\mathbf{B}}_m$ satisfy a homography $\mathbf{H} \in \Re^{3\times 3}$ as:

$$\bar{\mathbf{B}}_m = \mathbf{H}\bar{\mathbf{A}}_m. \quad (11)$$

Typically, RANSAC is a useful algorithm that removes outliers among the matches and be used to exploit $\mathbf{H}$ in (12). With the RANSAC algorithm, L sets of matched SCs are obtained after the outlier removal. Because the L matched SCs satisfy the relationship in (6), $\mathbf{H}$ can be expressed as:

$$\mathbf{H} = \begin{pmatrix} \mathbf{X}(\Delta\theta) & \mathbf{h} \\ \mathbf{0} & 1 \end{pmatrix} = \begin{pmatrix} \cos(\Delta\theta) & \gamma\sin(\Delta\theta) & \\ -\frac{1}{\gamma}\sin(\Delta\theta) & \cos(\Delta\theta) & \mathbf{h} \\ \mathbf{0} & & 1 \end{pmatrix}, \quad (12)$$

where $\mathbf{0} \in \Re^{1\times 2}$ is the zero-vector, and $\mathbf{h} \in \Re^{2\times 1}$ is the displacement vector induced by the difference between $\mathbf{O}_{C,1}$ and $\mathbf{O}_{C,2}$.

Here, it is noteworthy that, the determinant of $\mathbf{A}$ in (7) and $\mathbf{H}$ in (13) is always 1 in any condition. This implies that, if outliers are successfully removed and the matched SCs satisfy the homography in (13), the determinant of estimated homography should be nearly 1. Generally, RANSAC is composed of four major stages [20], however, to obtain the matched SCs, which satisfy the homography in (13), we propose an additional stage (*Step* 5) as follows:

(*Step* 1) Randomly select four components among the matches and compute the homography $\hat{\mathbf{H}}$ in (12) between the selected matches.

(*Step* 2) Judge whether other matches satisfy the relationship in (12) with the estimated $\hat{\mathbf{H}}$ in *Step* 1.

(*Step* 3) If a match satisfy the relationship in (12), add the match to the group of inliers. Keep the largest set of inliers.

(*Step* 4) Re-compute $\hat{\mathbf{H}}$ of the lease-squares on all of the inliers.

(*Step* 5) Compute the determinant of $\hat{\mathbf{H}}$ ($\det\left(\hat{\mathbf{H}}\right)$) and repeat the process in *Step* 1-5, until the determinant of the estimated homography approaches to 1 (i.e. $\left|\det\left(\hat{\mathbf{H}}\right) - 1\right| \le \varepsilon_0$).

Once the homography $\hat{\mathbf{H}}$ is given by the proposed RANSAC algorithm, RV of the target can be estimated by the trace of $\hat{\mathbf{H}}$:

$$\hat{\omega}_1 = \frac{1}{T_m}\cos^{-1}\left[\frac{\mathrm{tr}\left(\hat{\mathbf{H}}(\Delta\theta)\right) - 1}{2}\right]. \quad (13)$$

C. FINE RV ESTIMATION VIA SVD IN RC DOMAIN

After the aforementioned feature extraction and matching process, followed by SIFT, NNDR and RANSAC, we have L matched SCs, resulting in $\mathbf{P}_1 \in \mathbb{R}^{2\times L}$ and $\mathbf{P}_2 \in \mathbb{R}^{2\times L}$ in RD domain. Meanwhile, with the estimated $\hat{\omega}_1$ in (14), we can scale $\mathbf{P}_1$ and $\mathbf{P}_2$ into $\mathbf{P}_1^S$ and $\mathbf{P}_2^S$ in RC domain:

$$\mathbf{P}_1^S = \mathbf{S}\left(\hat{\omega}_1\right)\mathbf{P}_1, \quad \mathbf{P}_2^S = \mathbf{S}\left(\hat{\omega}_1\right)\mathbf{P}_2. \quad (14)$$

From (4), $\mathbf{P}_1^S$ and $\mathbf{P}_2^S$ have the following relationship:

$$\begin{aligned}\mathbf{P}_2^S &= \mathbf{R}(\Delta\theta)\mathbf{P}_1^S + \mathbf{S}\left(\hat{\omega}_1\right)\mathbf{O}_{C,1} - \mathbf{R}(\Delta\theta)\mathbf{S}\left(\hat{\omega}_1\right)\mathbf{O}_{C,2} \\ &= \mathbf{R}(\Delta\theta)\mathbf{P}_1^S + \mathbf{B}. \end{aligned} \quad (15)$$

In (16), the first term represents a rotation and the second term a translation component of $\mathbf{P}_1^S$. Typically, $\mathbf{B} = \mathbf{S}\left(\hat{\omega}_1\right)\mathbf{O}_{C,1} - \mathbf{R}(\Delta\theta)\mathbf{S}\left(\hat{\omega}_1\right)\mathbf{O}_{C,2}$ is the translation matrix induced by unknown ERCs of I_1 and I_2. To remove the effect of $\mathbf{B}$, we obtain new SCs, $\bar{\mathbf{P}}_1^c$ and $\bar{\mathbf{P}}_2^c$ in RC domain, by subtracting mean values of SCs in (18) from $\mathbf{P}_1^S$ and $\mathbf{P}_2^S$ (i.e. mean centering):

$$\bar{\mathbf{P}}_1^c = \mathbf{P}_1^S - \bar{\mathbf{P}}_1, \quad \bar{\mathbf{P}}_2^c = \mathbf{P}_2^S - \bar{\mathbf{P}}_2, \quad (16)$$

$$\bar{\mathbf{P}}_1 = \frac{1}{L}\sum_{i=1}^{L}\mathbf{p}_{1,i}^s, \quad \bar{\mathbf{P}}_2 = \frac{1}{L}\sum_{i=1}^{L}\mathbf{p}_{2,i}^s. \quad (17)$$

As a result, the newly mean-centered two sets of SCs, obtained from two sequential ISAR images in the RC domain, have only a rotation relationship as follows:

$$\bar{\mathbf{P}}_2^c = \mathbf{R}(\theta)\bar{\mathbf{P}}_1^c. \quad (18)$$

It is noteworthy that, (19) becomes an over-determined system with a rotation matrix $\mathbf{R}(\theta) \in \Re^{2\times 2}$ ($L \gg 2$). Then, its solution can be given by solving a least-square problem via SVD. To apply SVD, we compute the covariance matrix of $\bar{\mathbf{P}}_1^c$ and $\bar{\mathbf{P}}_2^c$ as follows:

$$\mathbf{C} = \bar{\mathbf{P}}_1^c\left(\bar{\mathbf{P}}_2^c\right)^T = \mathbf{U}\Sigma\mathbf{V}^T, \quad (19)$$

where $\mathbf{\Sigma} \in \Re^{2\times 2}$ is a diagonal matrix containing two singular values of $\mathbf{C}$, and $\mathbf{U} \in \Re^{2\times 2}$ and $\mathbf{V} \in \Re^{2\times 2}$ are orthogonal matrices containing right and left singular vectors, respectively. According to [21], rotation matrix $\mathbf{R}(\theta)$

between I_1 and I_2 can be obtained as the product of two orthogonal matrices, **U** and **V** as:

$$\mathbf{R}(\theta) = \mathbf{V}\mathbf{U}^T = \begin{bmatrix} \cos\theta & \sin\theta \\ -\sin\theta & \cos\theta \end{bmatrix}. \tag{20}$$

Consequently, the RV of the target can be re-estimated by the trace of $\hat{\mathbf{R}}(\theta)$ in (21):

$$\hat{\omega}_2 = \frac{1}{T_m}\Delta\hat{\theta} = \frac{1}{T_m}\cos^{-1}\left[\frac{1}{2}\mathrm{tr}\left(\hat{\mathbf{R}}(\Delta\theta)\right)\right]. \tag{21}$$

In this paper, RV of the target is evaluated twice ($\hat{\omega}_1$ and $\hat{\omega}_2$) in both RD domain and RC domain, respectively. Notably, as the matching accuracy of extracted SCs increases, the accuracy in RV estimation improves. Since the SCs after applying RASNAC algorithm is much precisely matched than the SCs after implementing NNDR, the better estimation accuracy of $\hat{\omega}_2$ than $\hat{\omega}_1$. The overall process of the proposed CRS scheme is illustrated in Fig. 2.

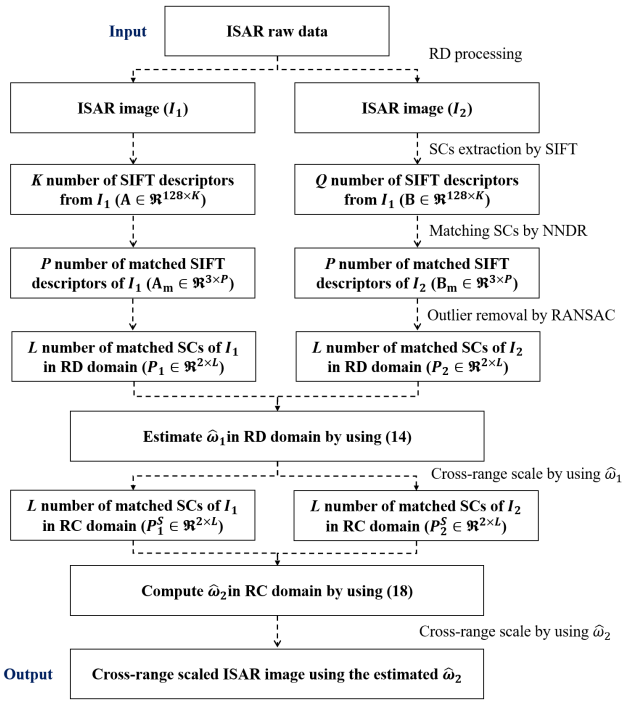

FIGURE 2. Overall flowchart of the proposed method.

D. COMPUTATIONAL COMPLEXITY

For a given ISAR raw data, two sequential ISAR images I_1 and I_2 can be obtained by RD processing. Suppose that, I_1 and I_2 are $M \times N$ images in the range and Doppler domain, the computational complexity of RD imaging requires $\Theta(M \log M) + \Theta(N \log N) = \Theta(M \log M)$. After applying SIFT algorithm, two data sets **a** and **b**, each of them contains K and Q number of SIFT descriptors of I_1 and I_2, respectively, can be obtained. Here, the computational complexity of **a** and **b** is proportional to$\Theta(MN + K) + \Theta(MN + Q) = \Theta(MN + K)$ [31]. In the proposed CRS scheme, the matching process of SCs between I_1 and I_2 consists of two steps: 1) NNDR and 2) RANSAC. In the former case, the complexity of NNDR requires $\Theta(KQD)$, mainly caused by the computation of euclidean distances, and D is the size of descriptor (i.e. $D = 128$ for SIFT). After conducting NNDR, L number of SCs are matched. In this case, the runtime of RANSAC can be expressed as [32]:

$$t_R = L\left(t_M + \bar{t}\right), \tag{22}$$

where t_M is the time needed for generating a hypothesis from a sampled data and $\bar{t}$ is the time for evaluating the hypothesis. It is noteworthy that, t_R increases as the number of sample (L) increases. Accordingly, RANSAC is notorious for high computational cost in the field of image processing. However, owing to the scattering mechanism of electromagnetic wave, major SCs in the ISAR image have much smaller number of samples than optical images. Moreover, as $M, N \gg K, Q > L$, the computational complexity of NNDR and RANSAC is much lower than that of

TABLE 2. Computational complexity.

Processing	Computation cost
Obtain I_1 and I_2	$\Theta(M \log M)$
Apply SIFT algorithm	$\Theta(MN + K)$
Apply NNDR	$\Theta(KQD)$, $D = 128$ *for SIFT*
Conduct RANSAC	$t_R = L(t_M + \bar{t})$
Compute SVD	$\Theta(l^3)$, $l = 2$ *for covariance matrix*
Total	$\approx \Theta(M \log M) + \Theta(MN + K)$

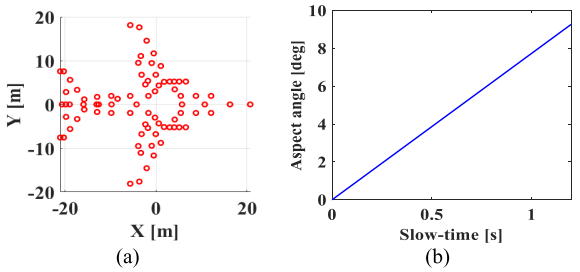

FIGURE 3. Simulation setup (a) point scatterer model, (b) target's RM.

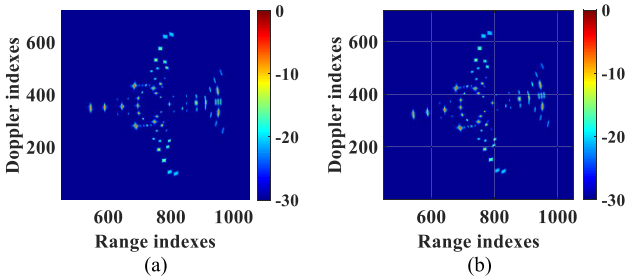

FIGURE 4. Two sequential RD images (a) I_1, (b) I_2.

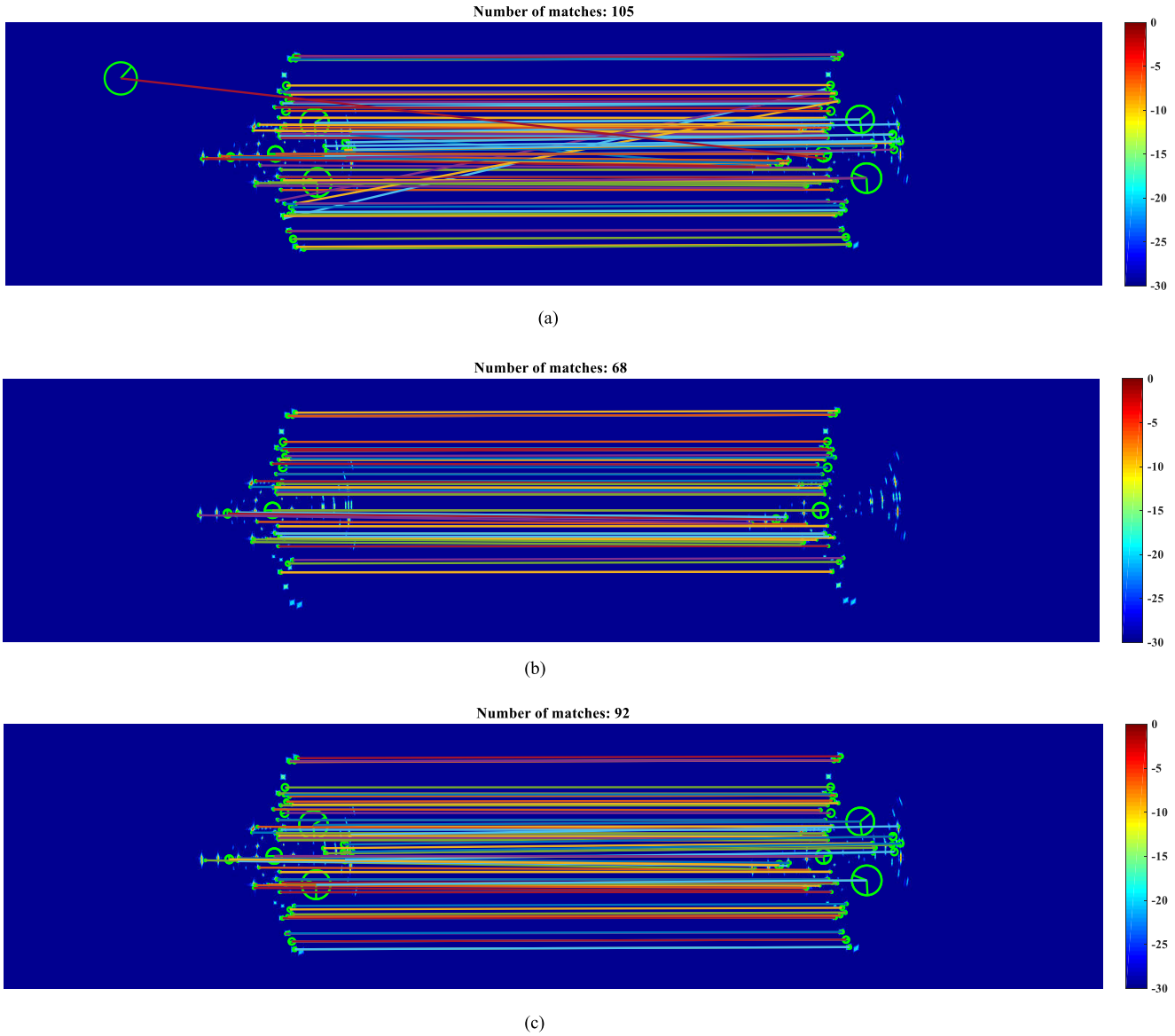

FIGURE 5. Matched SCs between I_1 and I_2 through (a) NNDR, (b) RANSAC when det (H) = 1.0792, (c) RANSAC when det(H) = 1.0001. Matched SCs are connected through lines. Circles are located at the position of extracted SCs on the image, and they denote the scale and orientation of descriptors.

RD imaging and SIFT algorithm. Consequently, the total computation cost of the proposed method is mainly determined by RD processing and SIFT.

IV. EXPERIMENTAL RESULTS

In this section, we verify the efficacy of the proposed method through both simulations based on the point scatter model and experiments using the real measured data. All computations were run by MATLAB in Windows 10 on an Intel Core i7-7700 CPU at 3.6 GHz.

A. SIMULATIONS

A Boeing 747-400 aircraft model composed of 88 isotropic SCs was used (Fig. 3. a). In simulations, we assumed a monostatic radar in the X-band with a stepped frequency waveform, and its specifications are as follows: carrier frequency 9 GHz, frequency bandwidth 500 MHz (i.e. 0.3 m range resolution), pulse repetition frequency (PRF) 400 Hz, and SNR = 20 dB. Target uniformly rotates with RV of 0.125 rad/s during CPI = 1.2 s, resulting in the RA of 8.6° (Fig. 3 b). During CPI, 480 pulses were received and they were equally divided to form two sequential ISAR images, I_1 and I_2. Hence, the time difference between I_1 and I_2 was 0.6 s. We exploited the conventional RD technique with zero-padding to obtain two sequential ISAR images in RD domain, and they had 1500 and 720 bins in the range and Doppler domain, respectively. As previously mentioned, ERC of the target is unknown in real-world ISAR imaging, and thus, we set the ERC as arbitrary position, randomly chosen in the RD domain (Fig. 4).

After applying SIFT algorithm, from I_1 and I_2, 196 and 182 SCs were extracted, respectively. Subsequently, NNDR and RANSAC described in Section III-A and III-B, were applied to the extracted SCs to match two sets of SCs. In Fig. 5, the NNDR produced the number of matched SCs as 105 and further, RANSAC reduced it by removing outliers. By comparing Fig. 5 (b) and (c), it can be noted that, traditional RANSAC algorithm successfully removes the outliers among the matches, nonetheless, the matched SCs do not satisfy the relationship in (4). On the other hand, matched SCs after conducting RANSAC algorithm with the additional step are robust to SC scintillations and have the rotation and scale relationship between I_1 and I_2. In this case, the estimated homography was $\hat{\mathbf{H}} = \begin{bmatrix} 0.9936 & -0.0542 & -0.5185 \\ 0.1092 & 1.0003 & 2.124 \\ -0.000 & 0.000 & 1.0000 \end{bmatrix}$, yielding the estimated RV $\hat{\omega}_1$ =0.1292 rad/s. By using $\hat{\omega}_1$, two sequential ISAR images in RD domain can be converted into those in RC domain as in (15). Then, rotation matrix $\mathbf{R}(\theta)$ and RV of the target can be re-estimated via SVD, (21) and (22), yielding $\hat{\mathbf{R}} = \begin{bmatrix} 0.9971 & 0.0759 \\ -0.0759 & 0.9971 \end{bmatrix}$, and $\hat{\omega}_2$ =0.1266 rad/s. Note that, the root mean square error (RMSE) of $\hat{\omega}_1$ and $\hat{\omega}_2$ were 3.36 % and 1.26 %, respectively. This implies that, the estimation accuracy was improved, and the two-step estimation resulted in an accurate RV estimation. The cross-range scaled ISAR image via proposed CRS scheme is illustrated in Fig. 6.

To validate the performance of the proposed method, we compared the existing CRS methods based on IBM approach [17], [18] with the proposed method. For the sake of notational brevity, the aforementioned methods will be referred to as PCA-CRS, and PSO-CRS, respectively. The received echoes have been contaminated by 100 independent noise realizations (i.e. Monte-Carlo simulations) for SNR ranges from -5 to 25 dB with a 5 dB increment. The RMSE between the true RV and the estimated one is illustrated in Fig. 7 (a).

As the SNR increases, the estimation accuracy was improved in all methods. Most notably, the proposed method maintains a good estimation accuracy even for low SNRs (below 5 dB). This implies that, owing to feature extraction and matching procedures, noise or scintillation of SCs hardly affected the estimation result of the proposed method. In contrast, the performance of PCA-CRS is significantly deteriorated at low SNRs, since the method has no matching procedures. Notably, as the rotation relationship between and I_1 and I_2 is directly exploited via RANSAC algorithm and SVD, the estimation accuracy of the proposed method is irrelevant to the number of matched SCs. In other words, as long as there is a rotation relationship between two sets of matched SCs, even with a small number SCs at low SNR, the proposed method can find an accurate RV of the target (Fig. 7 b). Furthermore, the proposed method exhibits robust estimation error against various RVs of the target and different SNRs (Fig. 8 a).

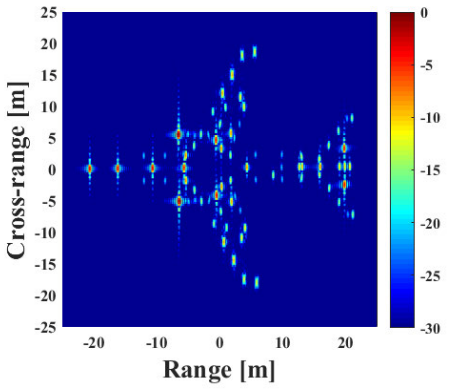

FIGURE 6. Rescaled ISAR image in RC domain.

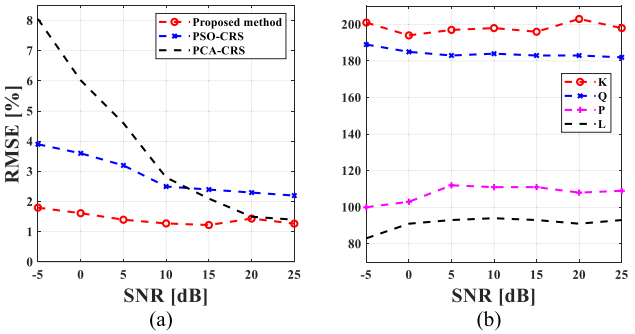

FIGURE 7. (a) Comparison of RMSE between true RV and estimates of various IBM approaches in different SNRs, (b) the number of features extracted via SIFT (*K*, *Q*) and the number of matched SCs after NNDR (*P*) and RANSAC (*L*).

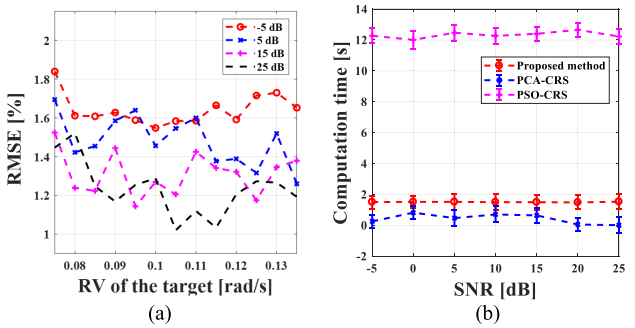

FIGURE 8. (a) RMSE in different RVs and SNRs by the proposed method, (b) comparison of computation time to existing methods at different SNRs.

In Fig. 8 (b), computation times for CRS methods are investigated. Each computation time was computed by averaging 100 Monte-Carlo simulations, as in Fig. 7. By adopting FAST and a suitable cost function, PCA-CRS has the best computational efficiency, while PSO-CRS consumes a huge amount of computation time owing to the iterations in PSO. Meanwhile, the computational efficiency of the proposed method is a little higher than that of PCA-CRS because the desired RV can be directly estimated by RANSAC algorithm and a simple SVD. As a result, proposed method has a good

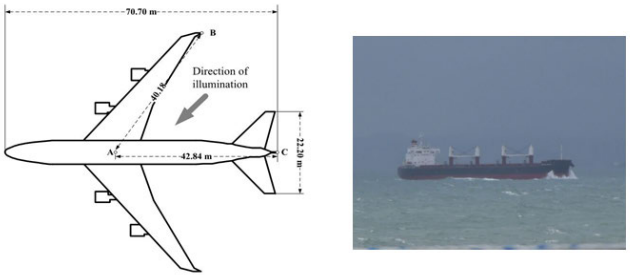

FIGURE 9. (a) Geometry of Boeing 747-400, and (b) an optical image of maritime target (a bulk carrier).

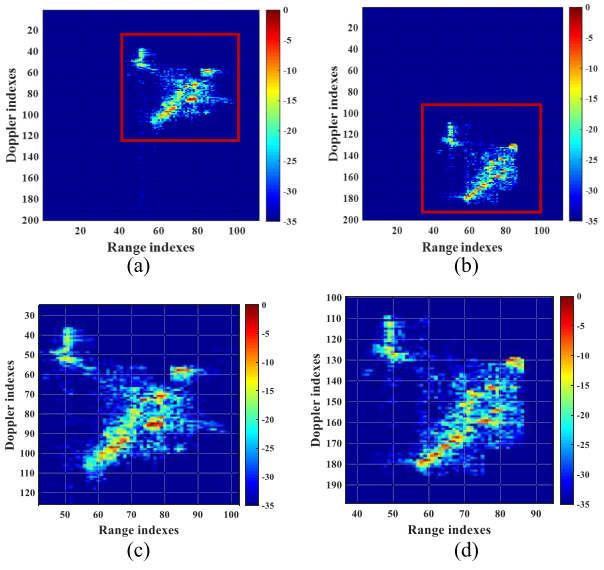

FIGURE 10. Two measured RD images of Boeing 747-400 (a) I_1, (b) I_2, (c) ISAR image corresponding to red square in (a), (d) ISAR image corresponding to red square in (b).

estimation accuracy as well as low computational complexity, compared to existing methods.

B. REAL MEASUREMENT

In this sub-section, the proposed method was applied to real data sets measured against both aircraft and maritime target (Fig. 9). In the former case, an X-band chirp pulse radar was installed at 3-km away from the aircraft, which was illuminated from the right rear. Specifications of the radar are as follows: carrier frequency 9.15 GHz, frequency bandwidth 100 MHz (i.e. 1.5 m range resolution), sampling rate 150 MHz, and PRF 500 Hz. During CPI=3 s, 1500 pulses were collected, and pulses in the 201-600 and 1101-1500 range were used to construct I_1 and I_2, as in Fig. 10. Moreover, owing to the rotating blades in the inlet of engine, the received signal was highly contaminated by the jet engine modulation. Thus, before applying the proposed method, an adaptive Gaussian representation [33] was adopted in advance to remove micro-Doppler components due to rotating blades.

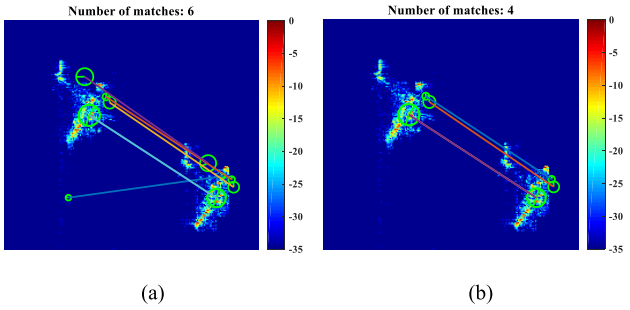

FIGURE 11. Matched SCs through (a) NNDR, (b) RANSAC. Matched SCs are connected through lines. Circles denote the SIFT descriptors.

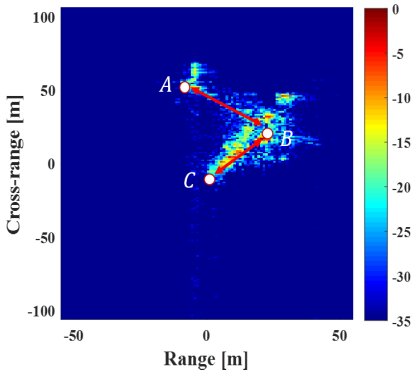

FIGURE 12. Rescaled ISAR image of Boeing 747-400.

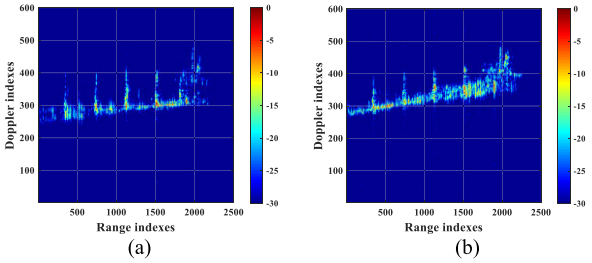

FIGURE 13. Two measured RD images of maritime target (a) I_1, (b) I_2.

In real-world ISAR imaging, the scintillation of SCs between two sequential ISAR images is significant, as shown in Fig. 10 (c) and (d). Nonetheless, after applying SIFT algorithm, we can extract 18 and 14 SCs from I_1 and I_2, respectively. Thereafter, matching between two sets of SCs has been performed through NNDR and RANSAC. In Fig. 11, the number of matched SCs was reduced from 6 to 4 via sequential combination of NNDR and RANSAC. Finally, the unknown rotation matrix of the target was obtained via (21) and (22): $\hat{\mathbf{R}} = \begin{bmatrix} 0.9995 & 0.0307 \\ -0.0307 & 0.9995 \end{bmatrix}$, yielding $\hat{\theta}$ =1.76 ° and $\hat{\omega}_2$ =0.0192 rad/s.

By using these estimates, we rescaled the ISAR image (Fig. 12). To investigate the accuracy of estimated values, we compared the length on the rescaled ISAR image with the real size of the target. In Fig. 12, we chose three points

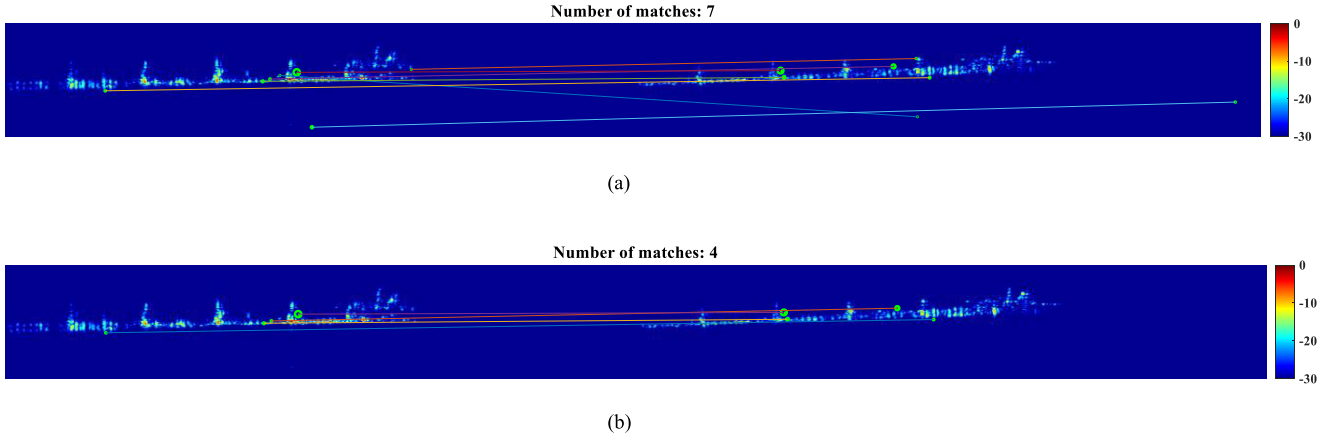

FIGURE 14. Matched SCs through (a) NNDR, (b) RANSAC. Matched SCs are illustrated in the same manner as in Fig. 5 and 11.

of the target: the tail (A), the center of the main body (B), and the right wing (C). The selected three points in the rescaled ISAR image corresponded to A= $[-7, 52.83]$ m, B= $[26, 25.08]$ m, and C= $[2, -8]$ m, leading to $\overline{AB} = 43.12$ m and $\overline{BC} = 40.87$ m. The measured lengths are very close to the true lengths in Fig. 9 (a), $\overline{AB} = 42.84$ m and $\overline{BC} = 40.18$ m. Besides, in [16] and [17], the validation of the methods were conducted to the same ISAR image (Fig. 11). According to [16] and [17], the estimated RV of the target was 0.019 rad/s, which is quite similar to the estimate of the proposed method, $\hat{\omega}_2$ =0.0192 rad/s.

In the case of maritime target (i.e. a bulk carrier), an X-band chirp pulse radar was installed on the shore, and echoes were collected from the target at a distance of 3.3 km. Specifications of the radar are as follows: carrier frequency 9.65 GHz, frequency bandwidth 200 MHz (i.e. 0.75 m range resolution), sampling rate 500 MHz, and PRF 8 kHz. During CPI=2.25s, 18000 pulses were received and pulses in the 1-12000 and 6001-18000 indexes were used to form two sequential ISAR images, I_1 and I_2 as shown in Fig. 13. As with the case of aircraft target, the fluctuation of amplitude between I_1 and I_2 (i.e. the scintillation of SCs) can be observed. The number of SCs obtained by SIFT was 982 in and 1364 in I_1 and I_2, respectively. However, after matching two sets of SCs, NNDR provided 7 matched SCs, and RANSAC reduced it to 4 (Fig. 14). Then, the matched SCs were exploited to estimate RV of the target via (21) and (22): $\hat{\mathbf{R}} = \begin{bmatrix} 0.9996 & 0.0277 \\ -0.0277 & 0.9996 \end{bmatrix}$, corresponding to $\hat{\theta}$ =1.58 ° and $\hat{\omega}_2$ =0.0369 rad/s. The ISAR image, which is rescaled by using $\hat{\omega}_2$, is illustrated in Fig. 15. In the image, two points (A and B) at the highest point on the pillar and bottom of the bulk carrier were selected. Contrary to the aircraft target, it was impossible to attain the exact specifications of the bulk carrier. Nonetheless, it is well-known that, most of the bulk carriers are in handysize and their height is nearly about 10 meters. Here, the points, A and B, were $[3320, 9.088]$ m, and $[3320, -0.5]$ m, resulting in the height between two points as $\overline{AB} \approx 9.6$ m.

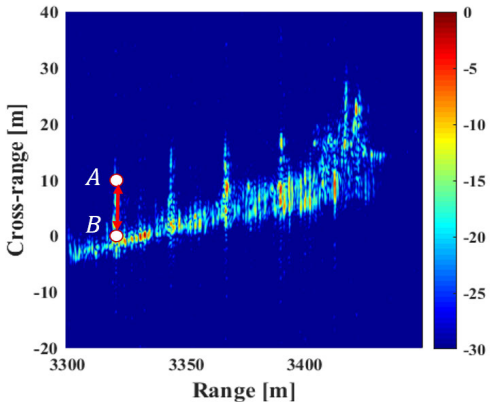

FIGURE 15. Rescaled ISAR image of maritime target.

Summarizing above experimental results, it is shown that, the proposed method demonstrated its robustness and effectiveness in not only simulations but also real measurements. Note that, the proposed method can estimate unknown RV of the target without any *prior* information of ERC, and thus, provide correctly-scaled ISAR images. Nonetheless, to address the accuracy of RV estimation in case of maritime targets, much research should be required.

V. CONCLUSION

In this paper, the scale and rotational relationship between two sequential ISAR images was analyzed first. Using this relationship, we proposed a new ISAR CRS method that estimates RV of a non-cooperative target based on two-step estimation, instead of an iterative searching process as in traditional CRS methods. The proposed method consists of two main steps. First, for the purpose of coarse RV estimation, SCs which are robust to scintillation between two sequential images were extracted and matched through SIFT and NNDR, respectively. Then, outliers were successfully removed with the proposed RANSAC algorithm. In this process, RV of the target was estimated a *priori* in RD domain. Second, by using the estimated RV in the previous step,

SCs in RD domain were scaled into those in RC domain, where SCs have only rotational relationship between them. Accordingly, we can estimate the rotation matrix by computing SVD of the covariance matrix of two sets of matched SCs, resulting in the precise estimation of RV of a target in RC domain. In this paper, to validate the effectiveness of the proposed method, experimental results of simulations and real measured data were provided. Thanks to the novel approach in the proposed CRS scheme, not only an accurate CRS can be achieved without a *prior* knowledge of ERCs of the target, but also it shows robust performance to the scintillation of SCs between two sequential ISAR images, which is the major problem of conventional CRS methods. In addition, the concept of the proposed method can be easily extended to various methods, regarding the estimation of angle between two sequential images.

REFERENCES

[1] C. Ozdemir, *Inverse Synthetic Aperture Radar Imaging With MATLAB Algorithms*. New York, NY, USA: Wiley, 2012.
[2] M. M. Menon, E. R. Boudreau, and P. J. Kolodzy, "An automatic ship classification system for ISAR imagery," *MIT Lincoln Lab. J.*, vol. 6, no. 2, pp. 289–308, 1993.
[3] D. Pastina and C. Spina, "Multi-feature based automatic recognition of ship targets in ISAR," *IET Radar, Sonar Navigat.*, vol. 3, no. 4, pp. 406–423, Aug. 2009.
[4] D. A. Ausherman, A. Kozma, J. L. Walker, H. M. Jones, and E. C. Poggio, "Development in radar imaging," *IEEE Trans. Aerosp. Electron. Syst.*, vol. AES-20, no. 4, pp. 363–400, Jul. 1984.
[5] V. C. Chen and M. Martorella, *Inverse Synthetic Aperture Radar Imaging: Principles, and Applications*. Raleigh, NC, USA: IET/Scitech, 2014.
[6] S.-J. Lee, M.-J. Lee, J.-H. Bae, and K.-T. Kim, "Classification of ISAR images using variable cross-range resolutions," *IEEE Trans. Aerosp. Electron. Syst.*, vol. 54, no. 5, pp. 2291–2303, Oct. 2018.
[7] M. Martorella, "Novel approach for ISAR image cross-range scaling," *IEEE Trans. Aerosp. Electron. Syst.*, vol. 44, no. 1, pp. 281–294, Jan. 2008.
[8] L. Liu, F. Zhou, M.-L. Tao, B. Zhao, and Z.-J. Zhang, "Cross-range scaling method of inverse synthetic aperture radar image based on discrete polynomial-phase transform," *IET Radar, Sonar Navigat.*, vol. 9, no. 3, pp. 333–341, Mar. 2015.
[9] S.-B. Peng, J. Xu, Y.-N. Peng, J.-B. Xiang, and X.-G. Xia, "Inverse synthetic aperture radar rotation velocity estimation based on phase slope difference of two prominent scatterers," *IET Radar, Sonar Navigat.*, vol. 5, no. 9, pp. 1002–1009, Dec. 2011.
[10] J. Sheng, M. Xing, L. Zhang, M. Q. Mehmood, and L. Yang, "ISAR cross-range scaling by using sharpness maximization," *IEEE Geosci. Remote Sens. Lett.*, vol. 12, no. 1, pp. 165–169, Jan. 2015.
[11] Y. Wang, X. Huang, and R. Cao, "Novel method of ISAR cross-range scaling for slowly rotating targets based on the iterative adaptive approach and discrete polynomial-phase transform," *IEEE Sensors J.*, vol. 19, no. 13, pp. 4898–4906, Jul. 2019.
[12] C. M. Yeh, J. Xu, Y. N. Peng, and X. T. Wang, "Cross-range scaling for ISAR based on image rotation correlation," *IEEE Geosci. Remote Sens. Lett.*, vol. 6, no. 3, pp. 597–601, Jul. 2009.
[13] F. Prodi, "ISAR cross-range scaling using a correlation based functional," in *Proc. IEEE Radar Conf.*, May 2008, pp. 1–6.
[14] S.-H. Park, H.-T. Kim, and K.-T. Kim, "Cross-range scaling algorithm for ISAR images using 2-D Fourier transform and polar mapping," *IEEE Trans. Geosci. Remote Sens.*, vol. 49, no. 2, pp. 868–877, Feb. 2011.
[15] Z. Xu, L. Zhang, and M. Xing, "Precise cross-range scaling for ISAR images using feature registration," *IEEE Geosci. Remote Sens. Lett.*, vol. 11, no. 10, pp. 1792–1796, Oct. 2014.
[16] S.-J. Jeong, B.-S. Kang, M.-S. Kang, and K.-T. Kim, "ISAR cross-Range scaling using radon transform and its projection," *IEEE Trans. Aerosp. Electron. Syst.*, vol. 54, no. 5, pp. 2590–2600, Oct. 2018.
[17] M.-S. Kang, J.-H. Bae, B.-S. Kang, and K.-T. Kim, "ISAR cross-range scaling using iterative processing via principal component analysis and bisection algorithm," *IEEE Trans. Signal Process.*, vol. 64, no. 15, pp. 3909–3918, Aug. 2016.
[18] B.-S. Kang, J.-H. Bae, M.-S. Kang, E. Yang, and K.-T. Kim, "ISAR cross-range scaling via joint estimation of rotation center and velocity," *IEEE Trans. Aerosp. Electron. Syst.*, vol. 52, no. 4, pp. 2023–2029, Aug. 2016.
[19] D. G. Lowe, "Distinctive image features from scale-invariant keypoints," *Int. J. Comput. Vis.*, vol. 60, no. 2, pp. 91–110, 2004.
[20] M. A. Fischler and R. Bolles, "Random sample consensus: A paradigm for model fitting with applications to image analysis and automated cartography," *Commun. ACM*, vol. 24, no. 6, pp. 381–395, 1981.
[21] D. W. Eggert, A. Lorusso, and R. B. Fisher, "Estimating 3-D rigid body transformations: A comparison of four major algorithms," *Mach. Vis. Appl.*, vol. 9, nos. 5–6, pp. 272–290, 1997.
[22] J. Wang and X. Liu, "Improved global range alignment for ISAR," *IEEE Trans. Aerosp. Electron. Syst.*, vol. 43, no. 3, pp. 12–17, Jul. 2007.
[23] T. Thayaparan, G. Lampropoulos, S. K. Wong, and E. Riseborough, "Application of adaptive joint time-frequency algorithm for focusing distorted ISAR images from simulated and measured radar data," *IEE Proc.-Radar, Sonar Navigat.*, vol. 150, no. 4, pp. 213–220, Aug. 2003.
[24] Y. Wang, H. Ling, and V. C. Chen, "ISAR motion compensation via adaptive joint time-frequency technique," *IEEE Trans. Aerosp. Electron. Syst.*, vol. 34, no. 2, pp. 670–677, Apr. 1998.
[25] S.-H. Lee, J.-H. Bae, M.-S. Kang, and K.-T. Kim, "Efficient ISAR autofocus technique using eigenimages," *IEEE J. Sel. Topics Appl. Earth Observ. Remote Sens.*, vol. 10, no. 2, pp. 605–616, Feb. 2017.
[26] J. Zheng, T. Su, W. Zhu, L. Zhang, Z. Liu, and Q. H. Liu, "ISAR imaging of nonuniformly rotating target based on a fast parameter estimation algorithm of cubic phase signal," *IEEE Trans. Geosci. Remote Sens.*, vol. 53, no. 9, pp. 4727–4740, Sep. 2015.
[27] J. M. Muñoz-Ferreras and F. Pérez-Martínez, "Uniform rotational motion compensation for inverse synthetic aperture radar with non-cooperative targets," *IET Radar, Sonar Navigat.*, vol. 2, no. 1, pp. 25–34, Feb. 2008.
[28] B.-S. Kang, B.-H. Ryu, C.-H. Kim, and K.-T. Kim, "Improved frame-selection scheme for ISAR imaging of targets in complex 3-D motion," *IEEE Sensors J.*, vol. 18, no. 1, pp. 111–121, Jan. 2018.
[29] M. Martorella and F. Berizzi, "Time windowing for highly focused ISAR image reconstruction," *IEEE Trans. Aerosp. Electron. Syst.*, vol. 41, no. 3, pp. 992–1007, Jul. 2005.
[30] M. Y. A. Gaffar, W. A. J. Nel, and M. R. Inggs, "Selecting suitable coherent processing time window lengths for ground-based ISAR imaging of cooperative sea vessels," *IEEE Trans. Geosci. Remote Sens.*, vol. 47, no. 9, pp. 3131–3140, Sep. 2009.
[31] P. Drews, R. de Bem, and A. de Melo, "Analyzing and exploring feature detectors in images," in *Proc. 9th IEEE Int. Conf. Ind. Informat.*, Jul. 2011, pp. 305–310.
[32] S. Choi, T. Kim, and W. Yu, "Performance evaluation of RANSAC family," in *Proc. Brit. Mach. Vis. Conf.*, 2009, pp. 1–12.
[33] J. Li and H. Ling, "Application of adaptive chirplet representation for ISAR feature extraction from targets with rotating parts," *IEE Proc.-Radar, Sonar Navigat.*, vol. 150, no. 4, pp. 284–291, Aug. 2003.

BO-HYUN RYU received the B.S. degree in electronic engineering from the Pohang University of Science and Technology (POSTECH), Pohang, South Korea, in 2015, where she is currently pursuing the Ph.D. degree with the Intelligent Radar System and Signal Processing Laboratory (IRAS). Her current research interests include radar imaging, radar signal processing and synthetic aperture radar (SAR), and inverse SAR (ISAR) imaging.

BYUNG-SOO KANG received the B.S. degree in electronic engineering from Yeungnam University, Gyeongsan, South Korea, in 2012, and the M.S. and Ph.D. degrees in electrical engineering from POSTECH, Pohang, South Korea, in 2014 and 2018, respectively. Since 2018, he has been with the Agency of Defense Development as a Senior Researcher. His current research interests include radar signal processing, synthetic aperture radar (SAR) imaging, inverse SAR (ISAR) imaging, and SAR calibrations.

MYUNG-JUN LEE received the B.S. degree in computer science and electrical engineering from Handong Global University, Pohang, South Korea, in 2014, and the M.S. and Ph.D. degrees in electrical engineering from POSTECH, Pohang, in 2017 and 2021, respectively. Since 2021, he has been with the Korea Aerospace Research Institute as a Senior Researcher. His current research interests include radar signal processing, satellite data service systems, and big-data systems.

KYUNG-TAE KIM (Member, IEEE) received the B.S., M.S., and Ph.D. degrees from POSTECH, Pohang, South Korea, in 1994, 1996, and 1999, respectively, all in electrical engineering. From 2002 to 2010, he was a Faculty Member with the Department of Electronic Engineering, Yeungnam University. Since 2011, he has been with the Department of Electrical Engineering, POSTECH, where he is currently a Professor. From 2012 to 2017, he served as the Director for the Sensor Target Recognition Laboratory, sponsored by the Defense Acquisition Program Administration and the Agency for Defense Development. Currently, he is the Director with the Unmanned Surveillance and Reconnaissance Technology (USRT) Research Center, and IRAS, POSTECH. He is the author of about 200 articles on journals and conference proceedings. His research interests include mainly in the field of radar signal processing and system modeling: SAR/ISAR imaging, target recognition, direction of arrival estimation, micro-Doppler analysis, automotive radars, digital beamforming, electronic warfare, and electromagnetic scattering. He was a recipient of several outstanding research awards and best paper awards from the Korea Institute of Electromagnetic Engineering and Science (KIEES) and international conferences. He is a member of KIEES. He is currently carrying out several research projects funded by the Korean Government and several industries.